JOURNAL OF GEOPHYSICAL RESEARCH, VOL. 112, A10311, doi:10.1029/2007JA012380, 2007

Observations of middle ultraviolet emissions in the middle and lower thermosphere: NO, O_2, O, and Mg^+

K. Minschwaner,[1] D. Herceg,[1] S. A. Budzien,[2] K. F. Dymond,[2] C. Fortna,[2,3] and R. P. McCoy[4]

Received 6 March 2007; revised 25 June 2007; accepted 12 July 2007; published 26 October 2007.

[1] We present an analysis of day and night limb spectra obtained from the Ionospheric Spectroscopy and Atmospheric Chemistry (ISAAC) satellite instrument in the middle ultraviolet spectral region between 260 and 300 nm. Tangent heights above the Earth's surface range from 81 to 200 km. These spectra contain signatures of daytime fluorescent scattering by nitric oxide in the γ bands, emission by atomic oxygen at 297.2 nm, and fluorescent scattering by ionized magnesium. The night spectra are dominated by the Herzberg bands of molecular oxygen. Our analysis includes retrievals for vertical profile densities of NO and slant column densities of O and Mg^+ in the lower thermosphere. We show how these quantities are related to variable inputs of solar soft X-ray and extreme ultraviolet radiation. The Herzberg band emission is used to constrain the ratio of Herzberg I to Herzberg II band emission and to determine the nighttime vibrational distribution of the excited $A^3\Sigma_u^+$ state of molecular oxygen.

Citation: Minschwaner, K., D. Herceg, S. A. Budzien, K. F. Dymond, C. Fortna, and R. P. McCoy (2007), Observations of middle ultraviolet emissions in the middle and lower thermosphere: NO, O_2, O, and Mg^+, *J. Geophys. Res.*, *112*, A10311, doi:10.1029/2007JA012380.

1. Introduction

[2] Atmospheric emission from the mesosphere and thermosphere in the middle ultraviolet (MUV) from 190 to 320 nm contains spectral features from excited states of several atomic and molecular species [e.g., *Meier*, 1991]. In the portion of the MUV between 260 and 300 nm, dayglow emissions include the strong nitric oxide (NO) γ band system, the N_2 Vegard-Kaplan (V-K) bands, and the OI 297.2 nm line [*Torr et al.*, 1993; *Cleary et al.*, 1995; *Bucsela et al.*, 1998]. In the upper mesosphere and lower thermosphere, dayglow emission can also be observed near 280 nm due to singly ionized magnesium [*Anderson and Barth*, 1971; *Gardner et al.*, 1995; *Dymond et al.*, 2003].

[3] The nighttime MUV emission in the upper atmosphere is dominated by the Herzberg I band system of molecular oxygen [*Hennes*, 1966; *McCoy*, 1983], along with the persistent oxygen 297.2 line. In contrast to many of the dayglow features, both of these emissions are confined to layer-like regions of the upper mesosphere and lower thermosphere between 90 and 105 km [*Sharp and Siskind*, 1989; *Siskind and Sharp*, 1991]. The Herzberg I nightglow also extends to longer wavelengths in the near ultraviolet from 310 to 400 nm, which allows for ground-based observations of this part of the Herzberg system [*Broadfoot and Kendall*, 1968; *Stegman and Murtagh*, 1991; *Slanger et al.*, 2004].

[4] Here we describe new observations of the terrestrial MUV dayglow and nightglow observed at moderate spectral resolution from space-borne instrumentation. This complements a previous study that focused on a different spectral region from the same instrument to determine the daytime NO distribution [*Minschwaner et al.*, 2004]. Analysis of these new data yields vertical profiles of the concentration of NO and slant column densities of oxygen and Mg^+ during the day. From night observations, we determine the vibrational distribution of O_2 A states between $v' = 4$ and 10.

2. Measurements and Analysis

[5] The Ionospheric Spectroscopy and Atmospheric Chemistry (ISAAC) instrument is a moderate resolution, ultraviolet limb imager on board the Advanced Research and Global Observing Satellite (ARGOS). ARGOS was launched on 23 February 1999, in a Sun-synchronous, near polar orbit at an altitude of 833 km. The ascending node, equatorial crossing time was approximately 0230 LT. The instrument platform scanned the Earth's limb between 81 and 750 km tangent height altitude, although useful data for the purposes of this study were limited to altitudes below about 200 km, as discussed below. The altitude resolution at the limb was about 7 km with an absolute tangent height uncertainty of ±4 km [*Minschwaner et al.*, 2004].

[6] Complete details of the ISAAC spectrometer and detector packages are given by *Wolfram et al.* [1999]. Here

[1]Department of Physics, New Mexico Institute of Mining and Technology, Socorro, New Mexico, USA.
[2]E. O. Hulburt Center for Space Research, Naval Research Laboratory, Washington, D. C., USA.
[3]Now at L. C. Wright, Inc., McLean, Virginia, USA.
[4]Office of Naval Research, Arlington, Virginia, USA.

0148-0227/07/2007JA012380$09.00

we briefly describe the instrument characteristics. The spectrograph employed a 3600 line/mm diffraction grating operated in first order. The spectral resolution ranged between 0.35 and 0.4 nm over the wavelength range 180 to 330 nm, which was divided into four overlapping passbands using a stepper motor that fixed the grating reflection angle in one of four positions. The NO study by *Minschwaner et al.* [2004] focused on passband 2 between 220 and 260 nm; here we focus on passband 3 between 260 and 300 nm, although the procedures for calibration and stray light removal are identical to those discussed in the previous study.

[7] Shown in Figure 1 is a daytime ISAAC spectrum from 20 October 1999, taken at a tangent height altitude of 88 km. Figure 1a shows the observed spectral intensity along with a solar irradiance spectrum from the SOLSTICE instrument [*Rottman et al.*, 1993] from the same time period. A number of adjustments are applied to the solar irradiances so that they may provide an accurate representation of the Rayleigh-scattered sunlight seen by ISAAC at tangent heights below about 110 km. First, the SOLSTICE irradiances are spectrally degraded by convolution with the ISAAC passband function in order to match the $\sim$0.4 nm resolution of ISAAC. Second, the shape of the SOLSTICE spectrum is tilted by a factor of λ^{-4}, normalized to one at 280 nm, to account for the Rayleigh scattering efficiency. Finally, the entire spectrum is multiplied by a single scale factor to match the ISAAC intensity between 286 and 287 nm, a region of the spectrum where there are no significant terrestrial emission features. This scale factor is calculated individually for every ISAAC spectrum. As can be seen in Figure 1, the daytime signal at these tangent altitudes is dominated by Rayleigh-scattered sunlight.

[8] Figure 1b shows the difference between the observed ISAAC intensity and the Rayleigh-scattered background based on SOLSTICE. This residual is attributed to dayglow emission that can be compared to a synthetic spectrum generated with the following components: part of the NO γ system containing the (1, 5), (0, 4), (1, 6), (0, 5), and (1, 7) vibrational bands, the atomic oxygen $O(^1S) \rightarrow O(^3P)$ transition at 297.2 nm, and the doublet lines of singly ionized magnesium at 279.6 and 280.3 nm. For the NO γ bands, the synthetic spectra are computed using rotational line emission rate intensities (g-factors) from *Stevens* [1995], appropriate for tangent altitude temperatures taken from the NRLMSISE-00 model [*Picone et al.*, 2002]. The relative intensities of the Mg^+ doublet lines are based on g-factors calculated by *Dymond et al.* [2003]. The agreement between the ISAAC observed dayglow and the calculated composite spectrum demonstrates that the instrument wavelength scale and calibration procedures are well characterized, and that the Rayleigh-scattered solar background can be effectively subtracted.

[9] A spectrum obtained at a higher tangent altitude of 123 km is shown in Figure 2. The neutral densities here are much lower and thus there is no need to account for Rayleigh solar scattering. A linear fit to mean intensities at 260, 275, and 287 nm is then used to remove any background residual that might arise from instrumental stray light or dark counts of the detector. We find good agreement between the observed and calculated dayglow spectrum at these higher tangent altitudes as well. Note that the synthetic spectrum contains components from the N_2 V-K bands as well as the features noted in Figure 1. The V-K spectrum is based on the AURIC radiance code [*Strickland et al.*, 1999] and it is spectrally degraded to match ISAAC's passband. In general, the V-K bands become apparent only above about 100 km. Comparison between Figures 2 and 1 also shows that the NO γ bands become relatively weaker at higher tangent altitudes, up to a factor of three between these two particular tangent heights. In the next section, we describe how these spectra are used to determine NO density profiles.

3. Nitric Oxide Results

[10] The ISAAC passband 3 data were used to determine NO $A^2\Sigma \rightarrow X^2\Pi$ γ band solar fluorescence intensities during an observation period between 15 October and 29 November 1999. NO concentrations for ISAAC passband 3 are retrieved using the integrated intensity of the NO $\gamma(1, 5)$ band located near 267 nm. This band was chosen for its relative brightness and for the lack of significant interference from any overlapping emission features. Both of these characteristics are apparent in Figures 1 and 2. Additionally, the (1, 5) band is not impacted by self-absorption because the lower electronic state involves the $v'' = 5$ level. The (1, 5) band intensity is determined by integrating ISAAC dayglow intensities between 266 and 268.5 nm. Observed band intensities are converted to slant column abundances of NO using temperature-dependent g-factors based on the calculations by *Stevens* [1995]. The $\gamma(1, 5)$ band g-factors integrated over this spectral interval are 1.481×10^{-6} photons s^{-1} at 200 K, decreasing to 1.265×10^{-6} photons s^{-1} at 1000 K.

[11] The vertical profile of NO concentration is calculated using a continuous set of limb scans that range between 81 and 158 km tangent height in steps of 7 km. The NO $\gamma(1, 5)$ band emission becomes too weak above 160 km to obtain useful NO measurements. NO slant columns at every tangent height are assumed to be the integrated result of spherically symmetric shells with uniform thickness, density, and temperature, and the retrieval employs matrix inversion techniques described by *McCoy* [1983]. Uncertainties in NO concentrations (1σ) are estimated using the root sum square of an overall calibration uncertainty of 25%, an uncertainty in the adopted g-factor of 7%, and the goodness of fit of the synthetic spectrum to the $\gamma(1, 5)$ band (typically between 5 and 10%).

[12] Figure 3 shows a vertical profile of NO from $\gamma(1, 5)$ band measurements, zonally averaged between 20°S and 20°N latitude and over a 4-d period from 26 November to 29 November. Also shown is a zonal mean NO profile measured over the following 4-d period 30 November to 3 December, obtained using ISAAC $\gamma(0, 1)$ band [*Minschwaner et al.*, 2004] intensities. It was not possible to observe both γ bands simultaneously since they are within different spectral passbands of the instrument. Nevertheless, this comparison of consecutive periods shows reasonable agreement between the two methods, with the $\gamma(1, 5)$ band retrieval showing larger NO near the peak values between 100 and 120 km. Smaller NO amounts are generally obtained from the $\gamma(1, 5)$ band measurements in

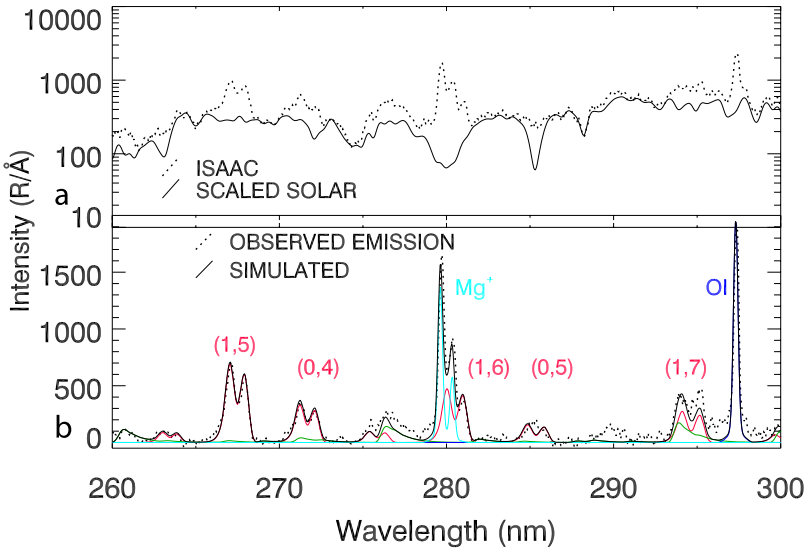

Figure 1. Ionospheric Spectroscopy and Atmospheric Chemistry (ISAAC) dayglow spectrum at 88 km tangent altitude from 20 October 1999, showing (a) calibrated spectrum (dotted) and scaled solar spectrum (solid) used to subtract Rayleigh-scattered sunlight and (b) the difference between the two curves from Figure 1a (dotted), along with the total simulated emission spectrum (solid). Individual components of the simulated spectrum are indicated for nitric oxide (red), ionized magnesium (light blue), nitrogen V-K (green), and atomic oxygen (dark blue).

the upper mesosphere, although the noise uncertainty is much higher there.

[13] Also shown in Figure 3 is the zonal mean NO over the 8-d period from the Student Nitric Oxide Experiment (SNOE) [*Barth et al.*, 2003; *Barth and Bailey*, 2004]. Agreement between all three profiles is good above 120 km. Between 105 and 115 km, SNOE observes more NO than either of the ISAAC retrievals, with a tendency for a narrower peak in concentration near 110 km. A large part of this discrepancy is related to the higher vertical resolution in SNOE data (~3 km) compared with ISAAC (~7 km). If the vertical resolution of the SNOE profile is degraded to correspond to ISAAC, then the peak NO values agree within the respective uncertainties. In addition, geophysical variability estimated from ISAAC is on the order of at least 30%, and could account for much of the difference as well. It should be noted that the discrepancy found previously between SNOE NO and ISAAC $\gamma(0, 1)$ band NO [*Minschwaner et al.*, 2004] is now reduced with SNOE V2.0 data, which adopts a g-factor that is 14% larger than used for SNOE V1.0 data [*Barth and Bailey*, 2004].

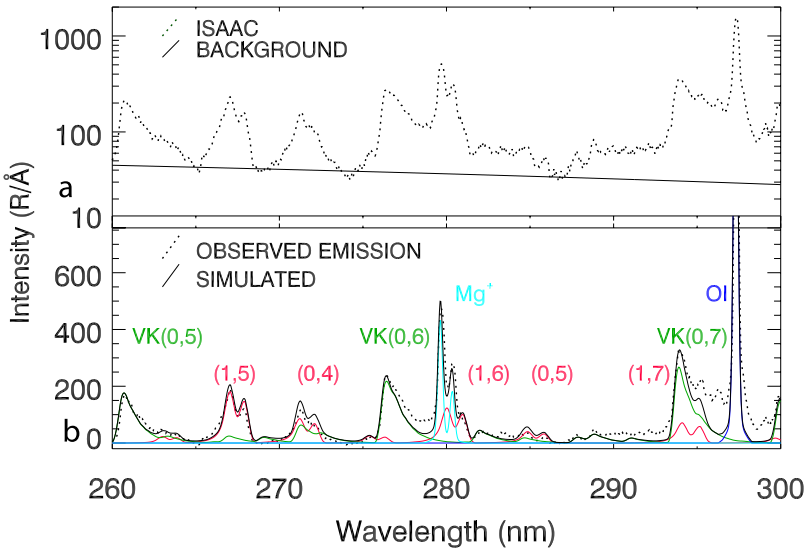

Figure 2. Same as Figure 1 but for a tangent altitude of 123 km. (a) At this higher altitude, the background (solid) was estimated from a linear fit to three minima in the dayglow spectrum (dotted). (b) Individual components of the simulated spectrum are the same as in Figure 1.

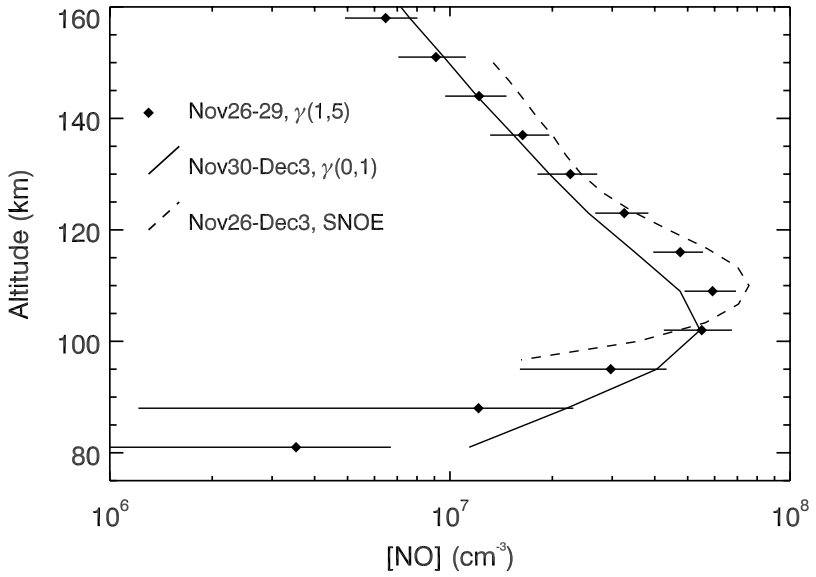

Figure 3. Mean of nitric oxide vertical profiles between ±20° latitude. Solid diamonds are ISAAC data analyzed here using the NO γ(1, 5) band during the period 26 November to 29 November 1999. Solid curve is obtained using ISAAC observations of the NO γ(0, 1) band from 30 November to 3 December 1999. Dashed curve is Student Nitric Oxide Experiment (SNOE) data, also based on the γ(0, 1) band, over the period 26 November to 3 December 1999.

[14] The new ISAAC γ(1, 5) values also confirm lower NO values in the middle thermosphere found earlier [*Minschwaner et al.*, 2004]. The reduced NO amounts support the argument for smaller O_2 densities than previously thought to exist in the middle and upper thermosphere, since the steady state concentration of NO is expected to be approximately proportional to the oxygen density [*Siskind et al.*, 2004]. These results are therefore consistent with reduced oxygen densities found in the NRLMSISE-00 empirical model [*Picone et al.*, 2002; *Siskind et al.*, 2004].

[15] The zonal mean distribution of NO measured on 26 October 1999 is shown in Figure 4a. Here, zonal averaging has been taken over geomagnetic latitude coordinates in order to highlight the effect of auroral production of NO at high latitudes [*Gerard and Barth*, 1977]. Auroral activity and solar fluxes on this day were both at relatively medium levels (K_p = 2.37, f10.7 = 187 (NOAA Space Environment Center (SEC), http://www.sec.noaa.gov, 2006)). The general distribution of NO shown in Figure 4 is typical of that found over the observation period, with maxima located between 100 and 110 km and between 60

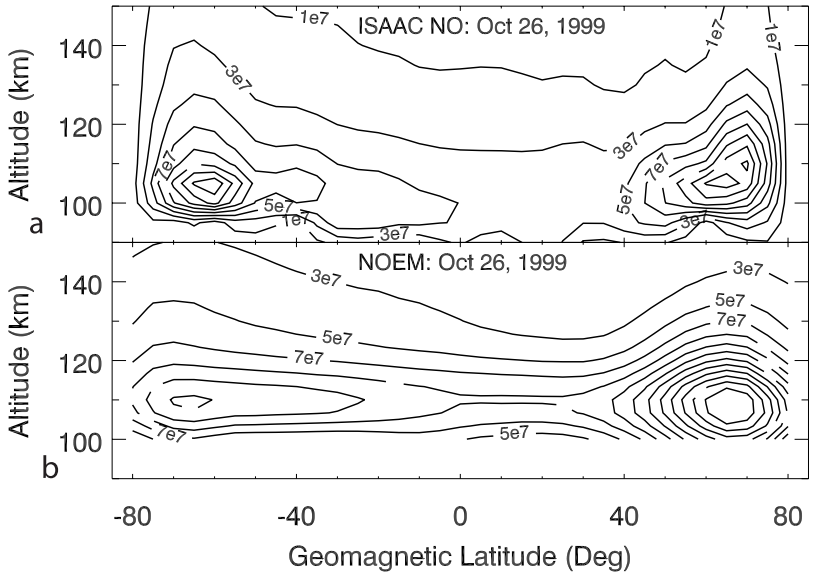

Figure 4. Comparison between (a) ISAAC passband 3 NO zonal mean distribution from 26 October 1999 and (b) results for the same day from the Nitric Oxide Empirical Model model.

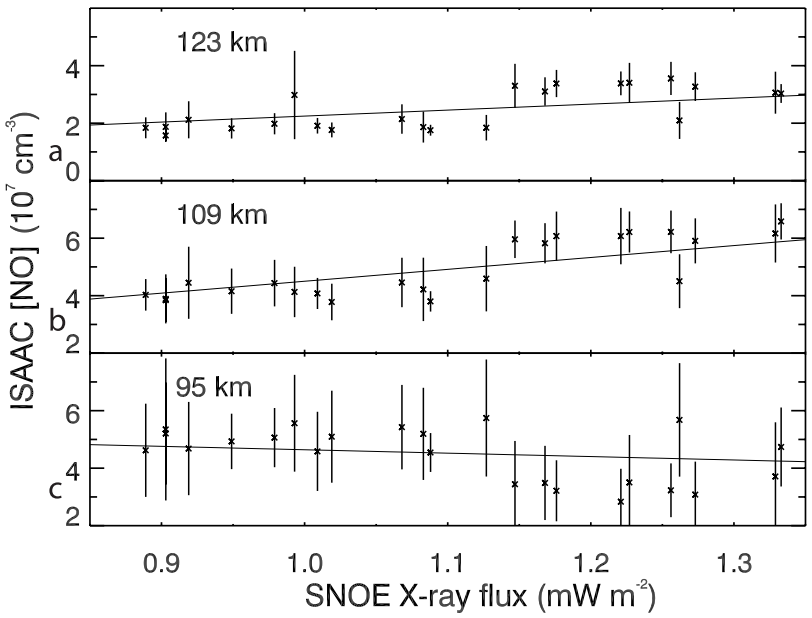

Figure 5. Daily mean NO concentrations between ±20° latitude at altitudes of (a) 123, (b) 106, and (c) 95 km, plotted versus daily mean solar X-ray flux (2−7 nm) measured by SNOE [*Bailey et al.*, 2000]. Solid lines indicate linear least squares fits.

and 70° geomagnetic latitude in both hemispheres. *Barth et al.* [2003] observed a similar emphasis on the auroral zones of both hemispheres from SNOE measurements.

[16] In Figure 4b, results are shown from the Nitric Oxide Empirical Model (NOEM) designed by *Marsh et al.* [2004] to represent the global thermospheric distribution of NO as a function of planetary magnetic index, day of year, and 10.7 cm solar radio flux. NOEM is based on an empirical orthogonal analysis of 935 days of SNOE observations. The morphology of NO is similar for ISAAC and NOEM, with NO maxima appearing at high latitudes in both hemispheres. In addition, both ISAAC and NOEM show the southern hemispheric maximum extending further to middle latitudes and a larger NO peak in the northern hemisphere. However, the hemispheric asymmetry is larger in NOEM and the overall NO densities are generally higher than for ISAAC (up to a factor of 2, e.g., at 40°N and 110 km). This latter feature is consistent with SNOE observing more NO above 100 km compared with ISAAC, as indicated from the profiles in Figure 3. We note also that the peak NO on average appears about 5 km lower in the ISAAC data compared with NOEM. Reasons for these differences are presently unclear.

[17] In contrast to high latitudes where the production of thermospheric NO is related primarily to ionization from precipitating auroral electrons, the low-latitude distribution of NO is thought to be controlled by the flux of solar soft X rays [*Siskind et al.*, 1995]. This link to the production of NO in the equatorial thermosphere has been confirmed by both SNOE [*Barth et al.*, 2003] and ISAAC passband 2 measurements [*Minschwaner et al.*, 2004]. In Figure 5 is shown the daily mean NO from ISAAC passband 3, averaged between 20°S and 20°N latitude and plotted as a function of daily mean solar X-ray flux from SNOE [*Bailey et al.*, 2000]. The resulting positive correlations are similar to those found previously [*Minschwaner et al.*, 2004], with the largest impact occurring at 109 km with a linear slope of 4.14 ± 0.14 (10^7 cm^{-3} NO) per (mW m^{-2} soft X-ray flux). There is a much smaller slope measured at 123 km, and very little correlation is found at 95 km. This altitude variation is similar to that obtained using ISAAC passband 2 data, but the slope at 109 km is about 25% smaller.

4. Ionized Magnesium

[18] As shown in section 2, ISAAC passband 3 spectra contain definite signatures of solar fluorescence from singly ionized magnesium, Mg^+. The doublet lines of Mg^+ near 280 nm overlap the same wavelength region as the NO γ(1, 6) band (Figures 1 and 2); however, since we are able to accurately account for the NO intensity based on the γ(1, 5) band, the relative contributions due to Mg^+ and NO can be effectively isolated. The fractional contribution due to NO typically ranges between 10% and 20%. To our knowledge, this is the first measurement of Mg^+ using the 280-nm dayglow lines that takes into account the overlap with NO fluorescence.

[19] Figure 6 shows spatial distribution of Mg^+ integrated line intensities for 18 October 1999, at a tangent height altitude of 102 km where the Mg^+ dayglow is generally the brightest. It will be shown below that the solar irradiances and geomagnetic activity for this day were relatively low compared with the rest of the observation period. The patchy nature of the Mg^+ emission seen in Figure 6 is typical for all observation days, and it is consistent with distribution of vertical column abundances retrieved from Nimbus 7 solar backscattered ultraviolet (SBUV) observations [*Joiner and Aiken*, 1996]. Previous measurements from space by *Mende et al.* [1985] and *Gardner et al.* [1995] have referred to these features as Mg^+ "clouds." We did not detect any tendencies for bright Mg^+ emission regions to cluster around any particular longitude or latitude.

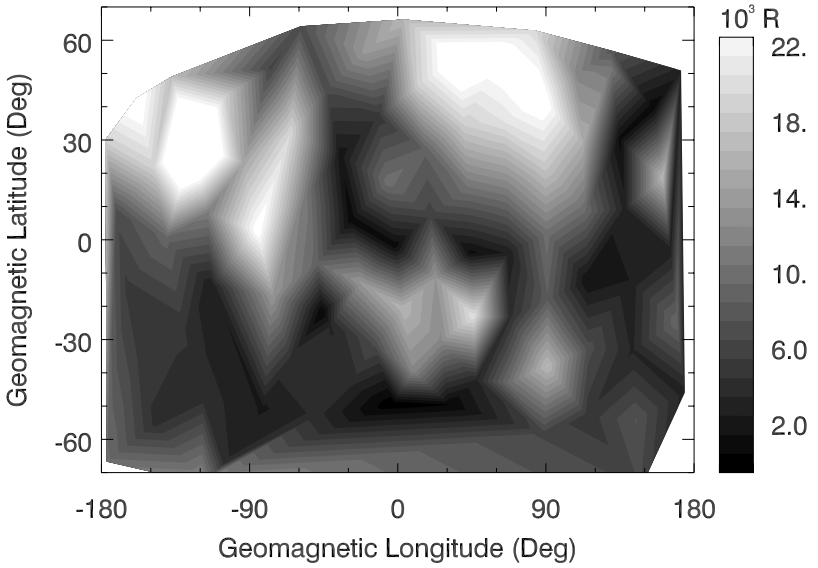

Figure 6. Intensity of Mg^+ emission at 102 km tangent height for 18 October 1999 versus geomagnetic longitude and latitude.

[20] The integrated line intensity observed at a given tangent height altitude is directly proportional to the line-of-sight slant column abundance of Mg^+. The proportionality constant, or g-factor, is adopted from the calculations by *Dymond et al.* [2003] to be 0.123 s^{-1} for the combined doublet. This value is slightly smaller than the g-factor of 0.128 s^{-1} calculated by *Anderson and Barth* [1971] and used in prior studies, due primarily to the different resolutions of solar spectral fluxes used in the two calculations. In addition, we adjust the g-factor to account for solar flux variability during the observing period. *Joiner and Aiken* [1996] showed that the solar spectral irradiance at the Mg^+ resonance varies approximately linearly with the SBUV MgII core-to-wing ratio, or MgII index. Their relationship is used to apply a time-dependent correction to the Dymond et al. g-factor of 1.35% per 0.001 change in MgII index, where the MgII index values are from the NOAA MgII Index [*Viereck et al.*, 2001].

[21] Figures 7 and 8 show the zonal mean distribution of Mg^+ slant column densities for 23 October and for 15 November, respectively. We find the largest column densities between about 90 and 100 km tangent altitude and generally no clear dependence on geomagnetic latitude between ±60° within this region of maximum Mg^+. However, on the topside of the layer between 100 and 140 km there is a tendency for larger Mg^+ near ±25° geomagnetic latitude, which may be related to transport processes within the lower and middle thermosphere [*Fesen et al.*, 1983]. The typically patchy nature of the Mg^+ distribution (Figure 6) calls into question the validity of retrieving concentrations from slant column densities by assuming homogeneous layer distributions, as was done previously

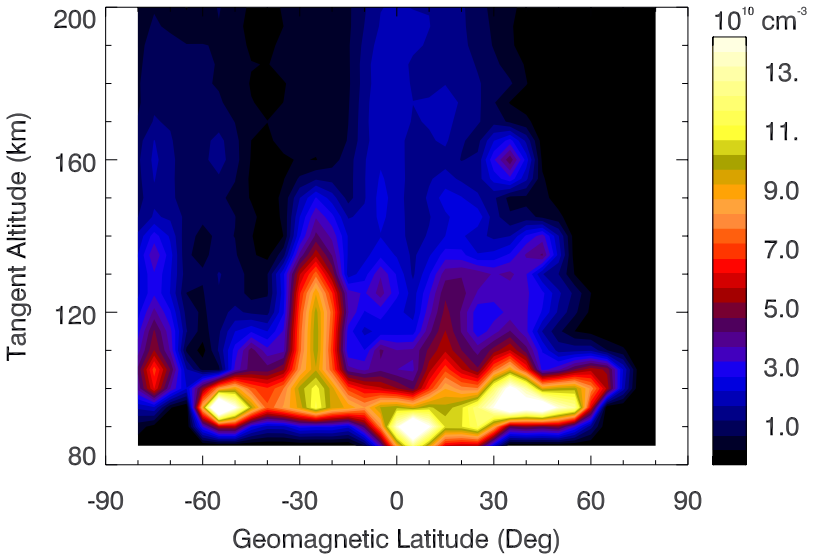

Figure 7. Zonal mean distribution of Mg^+ slant column densities observed on 23 October 1999.

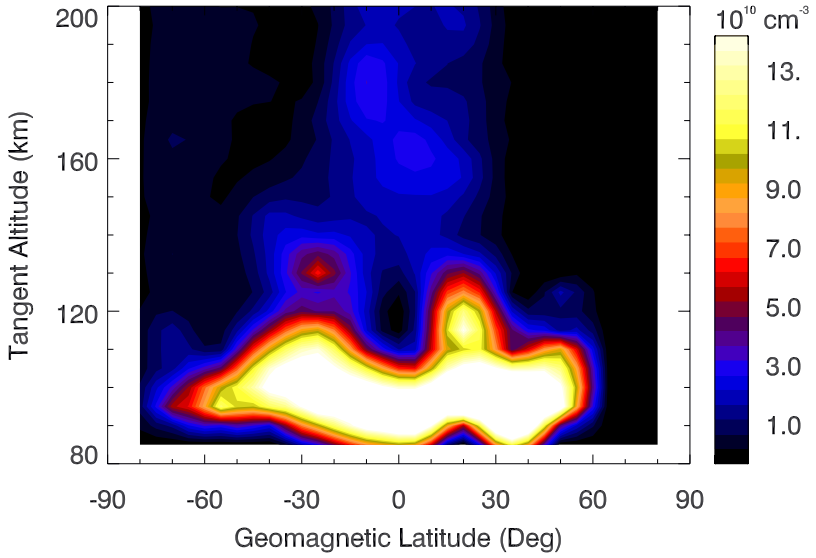

Figure 8. Same as Figure 7 but for 15 November.

for NO. Thus identification of these maxima in Mg^+ near ±25° geomagnetic latitude from single observing days should be considered tentative.

[22] Comparison of the Mg^+ column densities in Figures 7 and 8 shows larger overall amounts on 15 November than on 23 October. To investigate the temporal variations in Mg^+ over the observing period, we computed daily mean, "global" column amounts near the layer peak at 102 km tangent height and between ±60° geomagnetic latitude. Shown in Figure 9 is the time series of Mg^+, along with daily average values of the solar Lyman alpha line intensity measured by SOLSTICE [*Woods et al.*, 1996], and the Kp index of geomagnetic activity (NOAA SEC, http://www.sec.noaa.gov, 2006). The variation of mean Mg^+ appears better correlated with the solar Lyman alpha at 121 nm than with geomagnetic activity. This is likely related to corresponding variations in EUV irradiances which ionize NO and O_2; subsequent charge transfer reactions between neutral Mg and NO^+, O_2^+, are expected to be the dominant production mechanisms for Mg^+ [*Anderson and Barth*, 1971]. The time variations observed here thus appear to be dominated by variations in the source term rather than by transport or sinks.

[23] The timing of the Leonid meteor shower peak is indicated also in Figure 9 because meteor ablation is thought to constitute a major source for metals in the lower thermosphere and lower mesosphere [*Plane*, 2003]. The Leonid is one of the strongest showers and this particular event peaked around 0200 UTC on 18 November with a maximum zenith hourly rate of 5400 meteors per hour (American Meteor Society (AMS), http://www.amsmeteors.org, 2006). However, we find that the maximum mean Mg^+

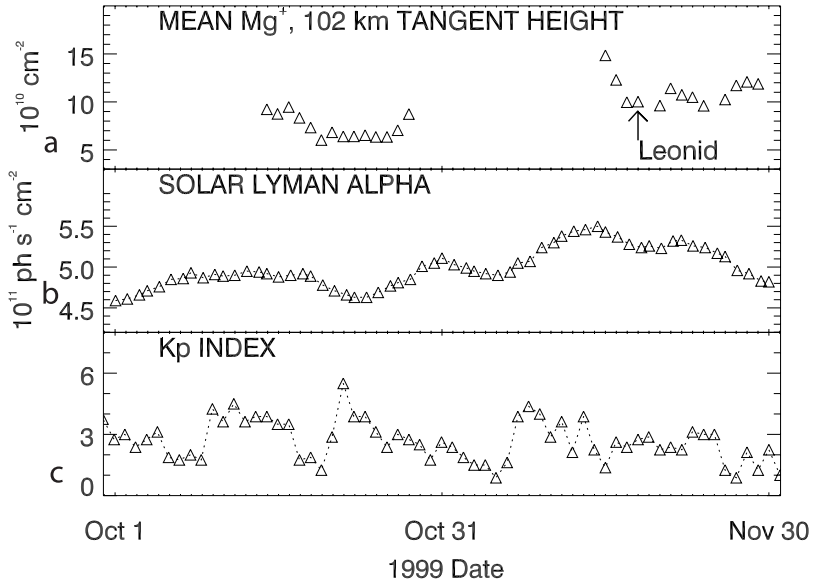

Figure 9. (a) Daily mean Mg^+ slant column density between ±20° latitude at tangent altitude of 102 km. Also shown are (b) the time series of solar Lyman α and (c) K_p index.

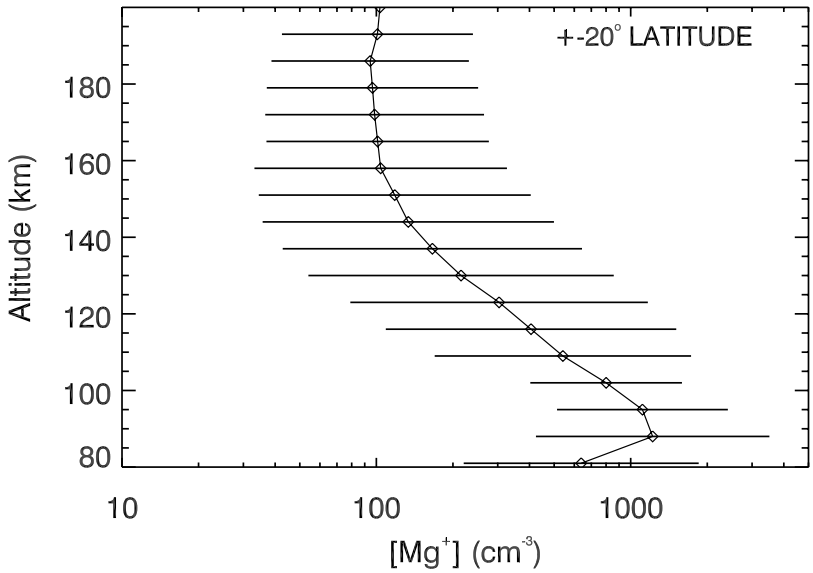

Figure 10. Mean vertical profile of Mg^+ constructed using all ISAAC passband 3 data from 15 October to 29 November between geomagnetic latitudes ±20°. Horizontal bars represent standard deviations based on the range of observed slant column amounts.

occurred 3 d prior to the Leonid shower peak (Figure 9; see Figure 8 for the corresponding Mg^+ distribution). A small impact cannot be discounted since postshower Mg^+ levels were generally higher than those measured 2 weeks prior, coupled with the fact that Leonid meteors were actually observed beginning on 15 November at a rate of 2–5 per hour (http://www.amsmeteors.org).

[24] The difficulties noted above in retrieving concentrations can be minimized by averaging all slant column amounts over the duration of the observing period between ±20° latitude. Figure 10 shows the resulting vertical profile of Mg^+ obtained from a standard inversion of the mean equatorial slant column amounts. Horizontal bars in Figure 10 represent relatively large ranges for the equatorial mean profile based on standard deviations of slant columns observed between ±20° latitude; this range is one measure of observed geophysical variability, although the noise contribution to the integrated line intensity (~5–10%) is not negligible here. The Mg^+ concentration at the layer peak near 90–95 km is slightly larger than 10^3 cm^{-3}, which is roughly a factor of 5 larger than the daytime equatorial rocket measurements reported by *Aiken and Goldberg* [1973]. The ISAAC Mg^+ decreases above about 95 km with a scale height of 20 km, reaching a near-constant value of 10^2 cm^{-3} between 140 and 200 km in agreement with the modeled results of *Fesen et al.* [1983]. In this region of the middle thermosphere, the ISAAC results are consistent with the range of 69–290 cm^{-3} estimated from space shuttle measurements using the GLO instrument [*Gardner et al.*, 1995]. Model-calculated daytime Mg^+ profiles from *McNeal et al.* [1996] are also in excellent agreement with the ISAAC profile over the entire altitude range, including the lower thermospheric peak. The vertical column abundance that corresponds to the profile shown in Figure 10 is 4.2×10^9 cm^{-2}, which is about 20% larger than the mean equatorial abundances observed using Nimbus 7 solar backscattered ultraviolet (SBUV) [*Joiner and Aiken*, 1996] during time periods when solar activity was similar to that for the ISAAC measurements.

5. Nightglow: Herzberg Bands

[25] The Herzberg bands of molecular oxygen are quite prominent in the nightglow MUV spectra from ISAAC. The peak emission occurs between 90 and 100 km in the lower thermosphere, corresponding to the maximum in production of the O_2 *A* state by atomic oxygen recombination. A daily zonal mean distribution of nightglow emission integrated over the Herzberg I (5, 3) band, between about 294 and 296 nm, is shown in Figure 11. We find a very sharp edge at about 110 km where the emission falls off rapidly with height. The latitude/height distribution is very similar to the integrated intensity of the oxygen 297.2 nm line. In fact, it has been shown that the ISAAC nightglow spectra display a constant ratio of Herzberg I(5, 3) to 297.2 nm emission, independent of latitude and tangent altitude [*Slanger et al.*, 2006]. Furthermore, it was found that the ratio of total Herzberg I emission to 297.2 nm emission was fixed at a value of 20.3 ± 3.1. *Slanger et al.* [2006] used these results, coupled with ground-based measurements of Herzberg I to oxygen 557.7 nm emission, to conclude that the ratio of radiative transition probabilities $O(^1S) \rightarrow O(^1D)$ to $O(^1S) \rightarrow O(^3P)$ is 9.8 ± 1.0 according to atmospheric observations. This ratio is lower than previous values between 18 and 24 measured in the laboratory and also lower than a branching ratio of 16 based on theory.

[26] In Figure 12 is shown an average of emission spectra obtained at 101 km and between -20 and 40° latitude. Also plotted is a synthetic spectrum calculated using a rotationally resolved model for the Herzberg I band emission. The model was constructed using O_2 FTS absorption measurements from *Yoshino et al.* [1994] for *A*-state term values and relative line branch strengths. Term values for the ground electronic state are based on spectroscopic constants from

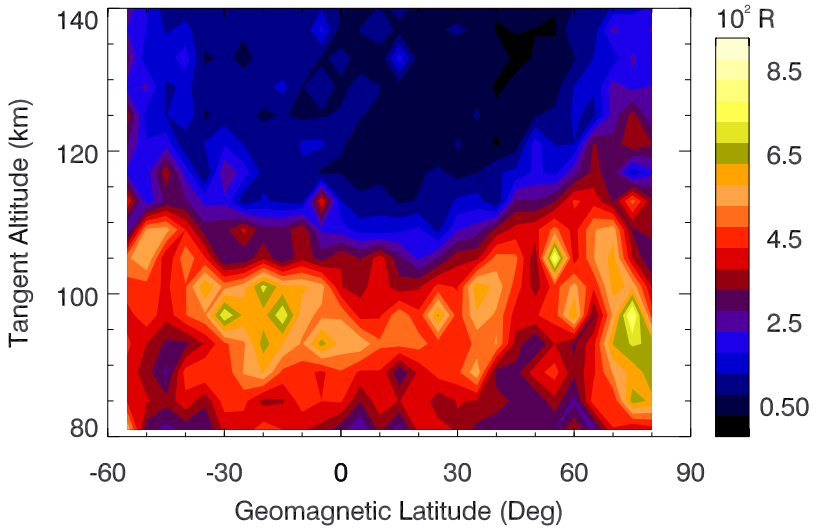

Figure 11. Zonal mean distribution of nightglow emission intensity in the O_2 Herzberg I (5, 3) band near 295 nm, observed on 27 November 1999.

Cheung et al. [1996]. The model contains 10 line branches including vibrational levels $v' = 4-11$ and $v'' = 0-5$ and rotational levels up to $N'' = 23$. The modeled line-by-line spectral grid is 0.03 cm^{-3} (the Doppler width at 190 K is approximately 0.06 cm^{-1}), and the results were degraded to match the spectral resolution of ISAAC (~0.4 nm at these wavelengths). Absolute band strengths for the Herzberg I system were adopted from the measurements by *Hasson et al.* [1970]. A preliminary estimate of the vibrational distribution of the *A* state was taken from the model results of *Siskind and Sharp* [1990] for high quenching. This distribution can alternately be retrieved from the ISAAC measurements, as discussed below.

[27] Herzberg II emission was included in the spectral model using a line-by-line analysis similar to that used for the Herzberg I system. The Herzberg II synthesis includes the R and P branches over the vibrational levels $v' = 1-12$ and $v'' = 0-5$, and rotational levels up to $N'' = 25$. Term values for the c state were based on the absorption measurements by *Ramsay* [1985] and transition probabilities were from *Bates* [1989]. The *c*-state vibrational distribution was adopted from *Slanger and Huestis* [1981]. This shape is similar to the *A*-state vibrational distribution from *Siskind and Sharp* [1990], but the peak is shifted by about 3 quanta to higher vibrational levels.

[28] We find good agreement between ISAAC observations and the spectral model of O_2 Herzberg nightglow

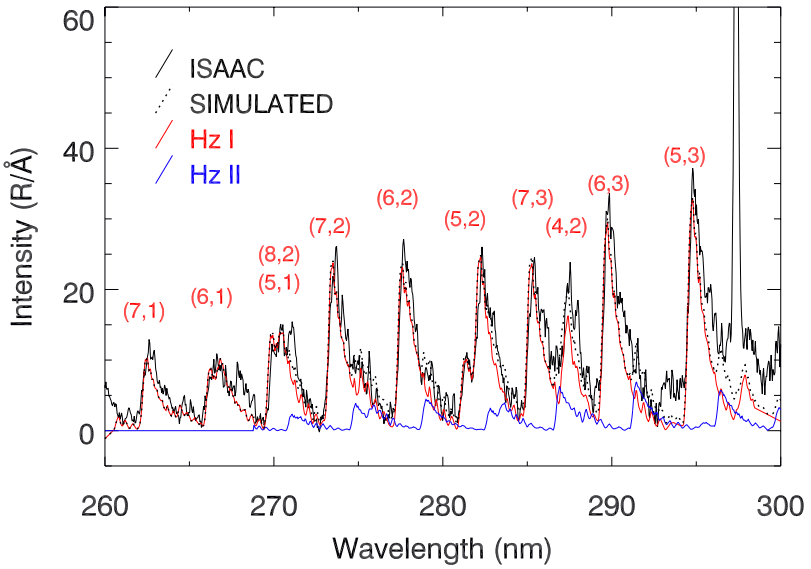

Figure 12. Mean Herzberg nightglow spectrum observed on 27 November 1999 between 0 and 40°N geomagnetic latitude and at a tangent altitude of 101 km. Dotted curve is the ISAAC observation and the black solid curve is a simulated spectrum. Components of the simulated spectrum are shown for the Herzberg I bands (red), Herzberg II bands (green), and atomic oxygen line (blue).

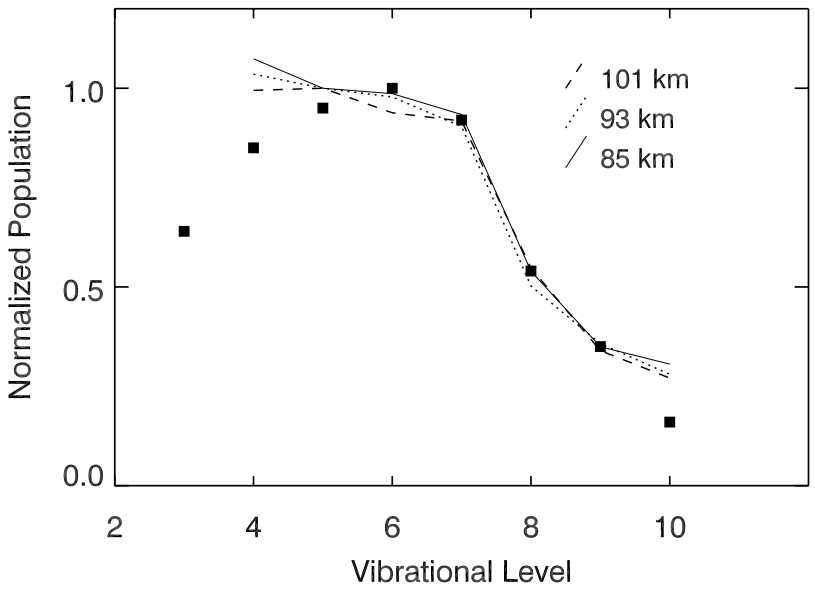

Figure 13. Vibrational distributions for the O_2 *A* state determined from ISAAC nightglow spectra at 85 km (solid), 93 km (dotted), and 101 km (dashed) tangent altitudes. All distributions are normalized to one at $v' = 5$. Also shown are values determined by *Slanger et al.* [2004] (solid squares).

(Figure 12). The impact of Herzberg II emission is most apparent for the (8, 2) and (7, 2) bands at 286.8 and 291.3 nm, respectively. The ratio of Herzberg I to Herzberg II emission in Figure 12 is 5.8 (range 4.5 to 8.5), with a large uncertainty arising from difficulties in distinguishing the Herzberg II bands above the detector noise in those spectral regions between the brighter Herzberg I features. Our values are generally lower than the value of 9:1 obtained by *Sharp and Siskind* [1989] from rocket measurements over roughly the same spectral interval. A smaller Herzberg I/Herzberg II ratio of 3 was measured by *Slanger and Huestis* [1981] at longer wavelengths from 310 to 450 nm. Most of the difference between ISAAC and the *Slanger and Huestis* ratio can be attributed to the different wavelengths ranges. In fact, they calculated an increased brightness of Herzberg I relative to Herzberg II emission (4:1) between 250 and 450 nm, implying that the ratio between 250 and 310 nm is larger than 4 and in reasonable agreement with ISAAC. *Eastes et al.* [1992] obtained a ratio of 4.8 based on nightglow observed from the S3-4 satellite at about 6 Å spectral resolution.

[29] The ISAAC ratio is also consistent with the range of values (3:1 to 6:1) from ground-based observations by *Stegman and Murtagh* [1991]. They also found that the Herzberg I to Herzberg II ratio appeared to increase with oxygen 557.7-nm line intensity, which supports the idea that the Herzberg II emission is proportional to the atomic oxygen density [O], in contrast to Herzberg I emission which is proportional to $[O]^2$. We might expect a similar behavior between the ISAAC ratio and oxygen 297.2-nm emission, since both atomic oxygen lines originate from the $O(^1S)$ state. However, the ISAAC data do not show any definitive relationship between the Herzberg I/Herzberg II ratio and oxygen 297.2-nm line intensity.

[30] Although the rotationally resolved Herzberg emission model should be capable of retrieving temperatures from observations at the spectral resolution of ISAAC, the signal to noise ratio is not sufficient for a reliably stable inversion. Instead, an a priori value of 190 K is used in the simulated spectrum, and this appears to be a reasonable choice based on comparisons with ISAAC. On the other hand, the vibrational distibution is reasonably well constrained by the ISAAC observations. Shown in Figure 13 is the mean vibrational distribution of the O_2 *A* state over the period of observations from Nov 22 to Nov 27. Three distributions are shown corresponding 85, 93, and 101 km tangent heights. These were determined using a least squares fit to the bands indicated in Figure 12. We note that the highest confidence is for the $v' = 5, 6, 7$ levels that contribute to bright, isolated band features. Higher uncertainties are involved for the $v' = 4, 8–10$ levels.

[31] The ISAAC *A*-state vibrational distributions shown in Figure 13 are consistent with the results from *Slanger et al.* [2004] obtained from ground-based astronomical sky spectra. Furthermore, the vibrational distribution is largely invariant with height, which is in agreement with previous ground-based and rocket measurements [*Murtagh et al.*, 1986; *Stegman and Murtagh*, 1991]. As discussed by *McDade and Llewellyn* [1986], the invariance of the *A*-state vibrational distribution favors relatively larger values for electronic quenching of this state relative to radiative emission. For example, comparison of the *A*-state vibrational distibution in Figure 13 with the model results of *Siskind and Sharp* [1990] would suggest a quenching rate constant with O_2 of at least 1.5×10^{-11} cm^3 s^{-1}. Laboratory measurements presented by *Slanger and Copeland* [2003] show even larger values for quenching of the $v' = 6–10$ levels with O_2, in the range 3 to 7×10^{-11} cm^3 s^{-1}.

6. Conclusion

[32] The ISAAC spectral data in passband 3 at wavelengths between 260 and 300 nm contain clear signatures of dayglow emission by nitric oxide, atomic oxygen, and

ionized magnesium in the lower and middle thermosphere. Analysis of the NO $\gamma(1, 5)$ band can be used to retrieve thermospheric densities. The nitric oxide vertical profiles are consistent with previous results from ISAAC using the NO $\gamma(0, 1)$ band, and they confirm a previous conclusion that supports reduced O_2 densities in the middle thermosphere contained in the NRLMSISE-00 empirical model [*Picone et al.*, 2002]. The distribution of NO from the ISAAC passband 3 analysis is also in agreement with the NOEM empirical model based on SNOE NO observations of the $\gamma(0, 1)$ band [*Marsh et al.*, 2004]. A positive correlation exists between equatorial NO in the lower thermosphere and the solar X-ray flux; however, the maximum slope of the linear correlation is smaller than found previously in ISAAC passband 2 data or in SNOE measurements [*Minschwaner et al.*, 2004; *Barth et al.*, 2003].

[33] The Mg^+ doublet emission near 280 nm overlaps with the NO $\gamma(1, 6)$ band, but retrieval of NO densities based on the $\gamma(1, 5)$ band allows the Mg^+ contribution to be effectively isolated. The brightest Mg^+ emission was observed within a layer between tangent heights of 90 and 100 km. Although the distribution of the layer maximum in geomagnetic latitude and longitude was typically patchy in nature, the average over all longitudes revealed no significant variations with respect to geomagnetic latitude. We found a significant response by Mg^+ to changing inputs of solar EUV, but very little effect from changes in K_p or to the input of Mg from the Leonid meteor shower. A vertical density profile constructed from the mean of all measurements showed maximum amounts of 1.2×10^3 cm^{-3} between 90 and 95 km, decreasing to about 10^2 cm^{-3} above 140 km.

[34] The ISAAC nightglow data were analyzed for O_2 Herzberg I and Herzberg II band emissions. This extends a previous analysis that showed a nearly constant ratio of O_2 Herzberg I to O 297.2-nm emission, one which implied a smaller branching ratio for $O(^1S \rightarrow {}^1D, {}^3P)$ emission than the current NIST recommendation [*Slanger et al.*, 2006]. The ISAAC observations also indicate a ratio of Herzberg I to Herzberg II intensity between 4.5 and 8.5. The vibrational population distribution of the *A*-state was found to agree well with the recent determination by *Slanger et al.* [2004], and the lack of any significant change in this distribution with tangent altitude or latitude points to relatively large values for electronic quenching of the *A* state by O_2.

[35] **Acknowledgments.** This research was supported by the Office of Naval Research, grant N00014031073. We thank Dan Marsh for supplying the NOEM model and for technical advice on its use, David Siskind and Michael Stevens for useful discussions on thermospheric nitric oxide, and Tom Slanger for the benefit of his extensive knowledge of the oxygen nightglow.

[36] Amitava Bhattacharjee thanks Tom Slanger and another reviewer for their assistance in evaluating this paper.

References

Aiken, A. C., and R. A. Goldberg (1973), Metallic ions in the equatorial ionosphere, *J. Geophys. Res.*, *78*, 734–745.

Anderson, J. G., and C. A. Barth (1971), Rocket investigation of the MgI and MgII dayglow, *J. Geophys. Res.*, *76*, 3723–3732.

Bailey, S. M., T. N. Woods, C. A. Barth, S. C. Solomon, L. R. Canfield, and R. Korde (2000), Measurements of the solar soft X-ray irradiance by the Student Nitric Oxide Explorer: First analysis and underflight calibrations, *J. Geophys. Res.*, *105*, 27,179–27,193.

Barth, C. A., and S. M. Bailey (2004), Comparison of a thermospheric photochemical model with Student Nitric Oxide Explorer (SNOE) observations of nitric oxide, *J. Geophys. Res.*, *109*, A03304, doi:10.1029/2003JA010227.

Barth, C. A., K. D. Mankoff, S. M. Bailey, and S. C. Solomon (2003), Global observations of nitric oxide in the thermosphere, *J. Geophys. Res.*, *108*(A1), 1027, doi:10.1029/2002JA009458.

Bates, D. R. (1989), Oxygen band system transition arrays, *Planet. Space Sci.*, *37*, 881–887.

Broadfoot, A. L., and A. R. Kendall (1968), The airglow spectrum 3100–10000 A, *J. Geophys. Res.*, *73*, 426–428.

Bucsela, E. J., D. D. Cleary, K. F. Dymond, and R. P. McCoy (1998), Atomic and molecular emissions in the middle ultraviolet dayglow, *J. Geophys. Res.*, *103*, 29,215–29,228.

Cheung, A. S.-C., K. Yoshino, J. R. Esmond, and W. H. Parkinson (1996), The Schumann-Runge absorption bands of O_2 at 670 K and the spectroscopic constants of the ground state X, *J. Molec. Spectrosc.*, *178*, 66–77.

Cleary, D. D., S. Gnanalingam, R. P. McCoy, K. F. Dymond, and F. G. Eparvier (1995), The middle ultraviolet dayglow spectrum, *J. Geophys. Res.*, *100*, 9729–9739.

Dymond, K. F., K. D. Wolfram, S. A. Budzien, A. C. Nicholas, R. P. McCoy, and R. J. Thomas (2003), Middle ultraviolet emission from ionized iron, *Geophys. Res. Lett.*, *30*(1), 1003, doi:10.1029/2002GL015060.

Eastes, R. W., R. E. Huffman, and F. J. LeBlanc (1992), NO and O_2 ultraviolet nightglow and spacecraft glow from the S3-4 satellite, *Planet. Space Sci.*, *40*, 481–493.

Fesen, C. G., P. B. Hays, and D. N. Anderson (1983), Theoretical modeling of low-latitude Mg^+, *J. Geophys. Res.*, *88*, 3211–3223.

Gardner, J. A., R. A. Viereck, E. Murad, D. J. Knecht, C. P. Pike, A. L. Broadfoot, and E. R. Anderson (1995), Simultaneous observations of neutral and ionic magnesium in the thermosphere, *Geophys. Res. Lett.*, *22*, 2119–2122.

Gerard, J. C., and C. A. Barth (1977), High latitude nitric oxide in the lower thermosphere, *J. Geophys. Res.*, *82*, 674–680.

Hasson, V., R. W. Nicholls, and V. Degen (1970), Absolute intensity measurements on the A-X Herzberg I band system of molecular oxygen, *J. Phys. B*, *3*, 1192–1194.

Hennes, J. P. (1966), Measurement of the ultraviolet nightglow spectrum, *J. Geophys. Res.*, *71*, 763–770.

Joiner, J., and A. C. Aiken (1996), Temporal and spatial variations in upper atmospheric Mg^+, *J. Geophys. Res.*, *101*, 5239–5249.

Marsh, D. R., S. C. Solomon, and A. E. Reynolds (2004), Empirical model of nitric oxide in the lower thermosphere, *J. Geophys. Res.*, *109*, A07301, doi:10.1029/2003JA010199.

McCoy, R. P. (1983), Thermospheric odd nitrogen 1. NO, N (^4S), and O (^3P) densities from rocket measurements of the NO δ and γ bands and the O_2 Herzberg I bands, *J. Geophys. Res.*, *88*, 3197–3205.

McDade, I. C., and E. J. Llewellyn (1986), The excitation of O (^1S) and O_2 bands in the nightglow: A brief review and preview, *Can. J. Phys.*, *64*, 1626–1630.

McNeal, W. J., S. T. Lai, and E. Murad (1996), A model for meteoric magnesium in the ionosphere, *J. Geophs. Res.*, *101*, 5251–5259.

Meier, R. R. (1991), UV Spectroscopy of the upper atmosphere, *Space Sci. Rev.*, *58*, 1–185.

Mende, S. B., G. R. Swenson, and K. L. Miller (1985), Observations of E and F region Mg^+ from Spacelab I, *J. Geophys. Res.*, *90*, 6667–6673.

Minschwaner, K., J. Bishop, S. A. Budzien, K. F. Dymond, D. E. Siskind, M. H. Stevens, and R. P. McCoy (2004), Middle and upper thermospheric odd nitrogen: 2. Measurements of nitric oxide from Ionospheric Spectroscopy and Atmospheric Chemistry (ISAAC) satellite observations of NO gamma band emission, *J. Geophys. Res.*, *109*, A01304, doi:10.1029/2003JA009941.

Murtagh, D. P., I. C. McDade, R. G. Greer, J. Stegman, G. Witt, and E. J. Llewellyn (1986), ETON-4 - An experimental investigation of the altitude dependence of the O_2 ($A^3\Sigma_u^+$) vibrational populations in the nightglow, *Planet. Space Sci.*, *34*, 811–817.

Picone, J. M., A. E. Hedin, D. P. Drob, and A. C. Aiken (2002), NRLMSIS-00 Empirical model of the atmosphere: Statistical comparison and scientific issues, *J. Geophys. Res.*, *107*(A12), 1468, doi:10.1029/2002JA009430.

Plane, J. M. C. (2003), Atmospheric chemistry of meteoric metals, *Chem. Rev.*, *103*, 4963–4984.

Ramsay, D. A. (1985), High-resolution studies of the near-ultraviolet bands of oxygen 1: The $c(^1\Sigma_u^-) - X(^3\Sigma_g^-)$ system, *Can. J. Phys.*, *64*, 717–720.

Rottman, G. J., T. N. Woods, and T. P. Sparn (1993), SOLar STellar Irradiance Comparison Experiment I: 1. Instrument design and operation, *J. Geophys. Res.*, *98*, 10,667–10,677.

Siskind, D. E., and W. E. Sharp (1990), A vibrational analysis of the O_2 Herzberg I system using rocket data, *Planet. Space Sci.*, *38*, 1399–1408.

Siskind, D. E., and W. E. Sharp (1991), A comparison of measurements of the oxygen nightglow and atomic oxygen in the lower thermosphere, *Planet. Space Sci.*, *39*, 627–639.

Siskind, D. E., D. J. Strickland, R. R. Meier, T. Majeed, and F. G. Eparvier (1995), On the relationship between the solar soft X ray flux and thermospheric nitric oxide: An update with an improved photoelectron model, *J. Geophys. Res.*, *100*, 19,687–19,694.

Siskind, D. E., J. M. Picone, M. H. Stevens, and K. Minschwaner (2004), Middle and upper thermospheric odd nitrogen: 1. A new analysis of rocket data, *J. Geophys. Res.*, *109*, A01303, doi:10.1029/2003JA009943.

Sharp, W. E., and D. E. Siskind (1989), Atomic emission in the ultraviolet nightglow, *Geophys. Res. Lett.*, *16*, 1453–1456.

Slanger, T. G., and R. A. Copeland (2003), Energetic oxygen in the upper atmosphere and the laboratory, *Chem. Rev.*, *103*, 4731–4766.

Slanger, T. G., and D. L. Huestis (1981), O_2 ($c^1\Sigma_u^- \rightarrow X^3\Sigma_g^-$) emission in the terrestrial nightglow, *J. Geophys. Res.*, *86*, 3551–3554.

Slanger, T. G., P. C. Cosby, D. L. Huestis, and A. M. Widhalm (2004), Nightglow vibrational distributions in the A and A′ states of O_2 derived from astronomical sky spectra, *Ann. Geophys.*, *22*, 3305–3314.

Slanger, T. G., P. C. Cosby, B. D. Sharpee, K. Minschwaner, and D. E. Siskind (2006), O(^{1}S $\rightarrow$ ^{1}D, ^{3}P) branching ratio as measured in the terrestrial nightglow, *J. Geophys. Res.*, *111*, A12318, doi:10.1029/2006JA011972.

Stegman, J., and D. P. Murtagh (1991), The molecular oxygen band systems in the U. V. nightglow: Measured and modelled, *Planet. Space Sci.*, *39*, 595–609.

Stevens, M. H. (1995), Nitric oxide γ band fluorescent scattering and self-absorption in the mesosphere and lower thermosphere, *J. Geophys. Res.*, *100*, 14,735–14,742.

Strickland, D. J., J. Bishop, J. S. Evans, T. Majeed, P. M. Shen, R. J. Cox, R. Link, and R. E. Huffman (1999), Atmospheric Ultraviolet Radiance Integrated Code (AURIC): Theory, software architecture, inputs, and selected results, *J. Quant. Spectrosc. Radiat. Transfer.*, *62*, 689–742.

Torr, D. G., M. R. Torr, and P. G. Richards (1993), Thermospheric airglow emissions: A comparison of measurements from ATLAS-1 and theory, *Geophys. Res. Lett.*, *20*, 519–522.

Viereck, R., L. Puga, D. McMullin, D. Judge, M. Weber, and W. K. Tobiska (2001), The MgII index: A proxy for solar EUV, *Geophys. Res. Lett*, *28*, 1343–1346.

Wolfram, K. D., K. F. Dymond, S. A. Budzien, C. B. Fortna, R. P. McCoy, and E. J. Bucsela (1999), The Ionospheric Spectroscopy and Atmospheric Chemistry Experiment on the Advanced Research and Global Observing Satellite: Quick look results, in *Ultraviolet Atmospheric and Space Remote Sensing: Methods and Instrumentation II*, edited by G. P. Carruthers and K. F. Dymond, *Proc. SPIE*, *3818*, 149–159.

Woods, T. N., et al. (1996), Validation of the UARS solar ultraviolet irradiances: Comparison with the ATLAS-1, -2 measurements, *J. Geophys. Res.*, *101*, 9541–9569.

Yoshino, K., J. E. Murray, J. R. Esmond, W. H. Parkinson, A. P. Thorne, R. C. M. Learner, and G. Cox (1994), Fourier transform spectroscopy of the Herzberg I bands of O_2, *Can. J. Phys.*, *72*, 1101.

S. A. Budzien and K. F. Dymond, E. O. Hulburt Center for Space Research, Naval Research Laboratory, 4555 Overlook Avenue, SE, Washington, DC 20375, USA.

D. Herceg and K. Minschwaner, Department of Physics, New Mexico Institute of Mining and Technology, Socorro, NM 87801, USA. (krm@kestrel.nmt.edu)

C. Fortna, MDNTB, 2611 Jefferson Davis Highway, Suite 700, Arlington, VA 22202, USA.

R. P. McCoy, Office of Naval Research, 875 North Randolph Street, Suite 1425, Arlington, VA 22203-1995, USA.